Electronic properties of thin $BaSi_2$ films with different orientations

2017 Jpn. J. Appl. Phys. 56 05DA03

(http://iopscience.iop.org/1347-4065/56/5S1/05DA03)

Japanese Journal of Applied Physics **56**, 05DA03 (2017)
https://doi.org/10.7567/JJAP.56.05DA03

PROGRESS REVIEW

Electronic properties of thin $BaSi_2$ films with different orientations

Dmitri B. Migas*, Vladislav O. Bogorodz, Anna V. Krivosheeva, Victor L. Shaposhnikov, Andrew B. Filonov, and Victor E. Borisenko

Belarusian State University of Informatics and Radioelectronics, 220013 Minsk, Belarus

*E-mail: migas@bsuir.by

Received September 6, 2016; accepted November 30, 2016; published online February 17, 2017

By means of ab initio calculations we have investigated surface energies and band structures of $BaSi_2$ thin films with (001), (010), (100), (011), (101), (110), and (111) surfaces. It is found that $BaSi_2$(111), (010), and (100) surfaces possess the smallest surface energies which are almost twice less than the ones of the other surfaces. All thin films with different orientations and thickness are shown to be semiconductors. The influence of quantum confinement effects on $BaSi_2$ thin film band gaps has been traced indicating nontrivial behavior because of the presence of surface states which characterize the top/bottom of the valence/conduction bands. By implementing a simple effective mass approximation model we could define energy positions of surface states for some $BaSi_2$ surfaces. © 2017 The Japan Society of Applied Physics

1. Introduction

Semiconducting silicides being well compatible with conventional silicon technology and promising for various applications are also known as environmentally friendly materials. Among them alkaline-earth silicides, namely Mg_2Si, Ca_2Si, and $BaSi_2$, have attracted much attention because they are already used in thermoelectric energy conversion[1)] and thin-film solar cells.[2)] Thus, barium dislicide ($BaSi_2$) with the band gap of 1.15–1.30 eV,[3,4)] rather large values of the absorption coefficient near the absorption edge,[5–8)] a large minority-carrier diffusion length[9,10)] in addition to a long minority-carrier lifetime[11,12)] can be viewed as a potential material for efficient conversion of sun's light to electricity.[2)] In fact, because of the marginal lattice mismatch (less than 1%) between the $BaSi_2$ and Si(111) planes, $BaSi_2$(100) thin films can be epitaxially grown on Si(111) substrates by molecular beam epitaxy and a n^+-$BaSi_2$/p^+-Si tunnel junction displaying very high photoresponsivity can be formed.[2,3)] However, it is suggested that there are a lot of defect levels at a such heterointerface indicating tunneling under a very small bias voltage to occur probably via the localized states in the forbidden gap rather than by band-to-band tunneling.[13,14)] Grain boundaries are reported to exist in thin films of $BaSi_2$ along with defect states associated with them.[15–17)] The latter ones can deteriorate electrical and optical properties of $BaSi_2$ films especially if they are used as a solar cell material. There is an experimental investigation of a surface structure of $BaSi_2$ films by using the coaxial impact-collision ion scattering spectroscopy and atomic force microscopy pointing out that $BaSi_2$(100) films on a Si(111) substrate are terminated by Si_4 tetrahedra.[18)] However, comprehensive knowledge of a $BaSi_2$ surface structure along with energy positions of surface states, which is still lacking, could help in optimizing a $BaSi_2$/Si heterojunction in order to achieve better performance of $BaSi_2$ thin-film based solar cells.

Since no theoretical work has been carried out to investigate different surfaces of $BaSi_2$, the main purpose of our brief review is to perform an analysis by means of ab initio calculations of surface energies and surface state energy positions for $BaSi_2$(001), (010), (100), (011), (101), (110), and (111) thin films. The influence of quantum confinement effects on band gaps in $BaSi_2$ films is estimated as well.

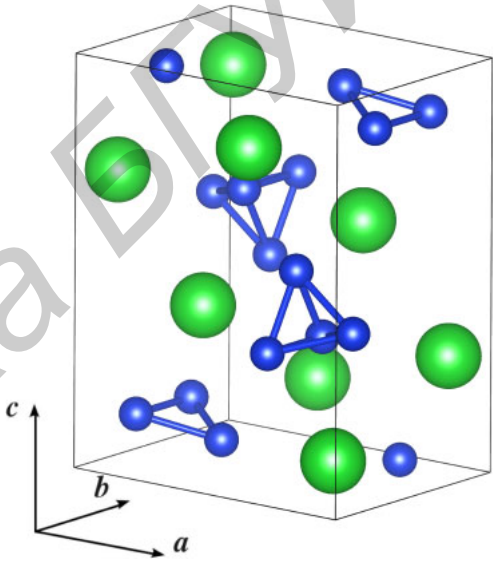

Fig. 1. (Color online) Unit cell of $BaSi_2$ in the simple orthorhombic structure. Large green spheres indicate Ba atoms, while small blue spheres stand for Si atoms. Lattice vectors are also shown.

2. Structural models and computational details

$BaSi_2$ crystallizes in a simple orthorhombic structure (the space group *Pnma*) with the following lattice parameters: $a = 8.942$ Å, $b = 6.733$ Å, and $c = 11.555$ Å.[19)] The unit cell contains eight Ba and sixteen Si atoms where the latter ones form slightly distorted and isolated Si_4 tetrahedra (as can be seen in Fig. 1) while Ba atoms help to guide orientation of the tetrahedra.[19)] In addition, both Ba and Si atoms in the unit cell are grouped into two and three sets of chemically inequivalent sites, respectively.[19)]

In order to study surfaces of $BaSi_2$, we have formed slabs with two equal surfaces by stacking several unit cells along a specific orientation to get a desirable slab thickness. For $BaSi_2$(001), (010), and (100) slabs the common simple orthorhombic unit cell can be used whereas for $BaSi_2$(011), (101), (110), and (111) slabs it is necessary to choose the other ones which are monoclinic or even triclinic. We have considered the slabs up to 7–12 nm in thickness and with the 1×1 surface reconstruction. For all cases the $BaSi_2$ stoichiometry was kept invariable.

The structural optimization and electronic band structure calculations of $BaSi_2$ thin films with different orientations have been performed by utilizing the first principles total energy projector-augmented wave method (code VASP) described in detail elsewhere.[20–23] Exchange and correlation potentials were included using the generalized gradient approximation of Perdew–Burke–Ernzerhof.[24] The $BaSi_2$(001), (010), (100), (011), (101), (110), and (111) thin films have been considered as periodic arrangement of slabs separated by 11 Å of vacuum. This thickness of vacuum is found to be enough to exclude an interaction between the slabs. All atoms in a slab were allowed to relax. The energy cutoff was set to 280 eV. To assure convergence with respect to **k**-points, the $9 \times 9 \times 1$ grid of Monkhorst–Park points has been used at final iterations. The atomic relaxation was stopped when forces on the atoms were smaller than 0.05 eV/Å. The convergence in the total energy was better than 1 meV per formula unit. The calculations of band structures were performed on the self-consistent charge densities. We applied the linear tetrahedron method with Blöchl corrections for a Brillouin-zone integration and for calculations of the total density of states. The surface energies of various $BaSi_2$ surfaces have been calculated as a difference in the total energy between a slab and the bulk (rescaled to the number of formula units as in the corresponding slab) divided by doubled surface area. The charge distributions and transfers between atoms have been analyzed by implementing the Bader method.[25] In the case of bulk calculations the same settings have been used except for $7 \times 9 \times 7$ grid of Monkhorst–Park points.

3. Results and discussion

3.1 Structural optimization

Top and lateral views of $BaSi_2$ slabs with (001), (010), (100), (011), (101), (110), and (111) surfaces are shown in Fig. 2 indicating that all Si_4 tetrahedra are preserved at the surface as experimentally observed in Ref. 18 for the $BaSi_2$(100). After full structural optimization the $BaSi_2$(100) and (111) surfaces possess Ba atoms as topmost atoms while, on the contrary, Si atoms of complete Si_4 tetrahedra terminate the $BaSi_2$(110) surface. For the other $BaSi_2$ surfaces both Ba and some Si atoms can be considered as topmost atoms (see corresponding lateral views in Fig. 2). Moreover, we have revealed that surface atoms displayed inward relaxation leading to slight reduction in slab thickness. Si–Si interatomic distances in Si_4 tetrahedra at the surface (2.34–2.46 Å) differed from the ones in the bulk (2.41–2.44 Å) while in an inner part of the slabs they were very close. However, this issue was not so pronounced for the tetrahedra at the $BaSi_2$(100), (010), and (111) surfaces where Si–Si interatomic distances were not significantly distorted. Some changes in Ba–Si interatomic distances can be spotted as well and such distances get shorter mainly for surface atoms (compare 3.29 and 3.39 Å).

The Bader analysis of charge transfer between atoms in the $BaSi_2$ bulk has revealed that each Si atom accepts 0.5–0.7e^- while Ba atom donates 1.24–1.25e^-. Moreover, the appearance of Si_4 tetrahedra suggests that they can be considered as Zintl $[Si_4]^{2.49-}$ anions and $[Ba_2]^{2.49+}$ correspondingly can be treated as cations. Similar issue has been already observed for $BaGe_2$ and $SrGe_2$, which are isostructural to $BaSi_2$, and the covalent nature of chemical bonding between Ge atoms is found in the Ge_4 tetrahedra.[26] Thus, Si_4 or Ge_4 tetrahedra acting as anions additionally attract charge from Ba or Sr atoms indicating the presence of a sizable ionic contribution to chemical bonding. For the $BaSi_2$(010), (100), and (111) slabs we have traced no significant charge variation in Si_4 tetrahedra with respect to the bulk case. Even the tetrahedra located at the surface have around $-2.50e^-$. Only the topmost Si atoms can attract less charge ($\sim 0.34e^-$) however it is immediately counterbalanced by the other Si atoms in the tetrahedron. In the case of the $BaSi_2$(001), (011), (101), and (110) slabs the topmost Si atoms have even less negative charge of $0.15e^-$ that leads to smaller total charge of $\sim 2.37e^-$ per a $[Si_4]$ anion. Contrary to Si atoms, Ba atoms donate almost the same amount of charge (1.21–1.28e^-) independently of their location in a slab.

The calculated $BaSi_2$ surface energies, which are summarized in Table I, clearly indicate that (111), (010), and (100) surfaces possess the smallest values. These values are even smaller than for Ca_2Si and Mg_2Si surfaces[27,28] in addition to different Si and Ge surfaces.[29] Our attempts to construct surfaces with broken tetrahedra having less Si atoms resulted in sizable increasing of surface energy. Thus, the experimental observation that the $BaSi_2$(100) films are terminated by complete Si_4 tetrahedra[18] seems to be typical of any $BaSi_2$ surface. To this end we can link values of surface energy and charge transfer between atoms to a type of topmost atoms. In fact, if Ba atoms act as topmost atoms [the cases of the $BaSi_2$(100) and (111) surfaces], the corresponding $BaSi_2$ surfaces possess the smallest values of surface energies, the least distorted Si–Si interatomic distances and almost the same charge accumulation among Si atoms in surface tetrahedra. At variance with these cases, for the $BaSi_2$(001), (011), and (110) surfaces topmost Si atoms cannot efficiently attract charge from Ba atoms leading to significant distortion in Si–Si interatomic distances in tetrahedra because the other Si atoms gain much more charge in order to maintain the same charge balance per tetrahedra unavoidably leading to dipole formation within a tetrahedron and to reduction in the Si–Si bond length. In turn, it provides an increase in the surface energy. It should be noted here that for the most stable surfaces of Ca_2Si and Mg_2Si the metal atoms are also on the top.[27,28]

3.2 Band structure

The corresponding band diagrams of $BaSi_2$ slabs with thickness of about 5 nm and different surfaces are shown in Fig. 3. It is evident that all slabs are mainly indirect band-gap semiconductors. Only the $BaSi_2$(111) slab is characterized by the direct transition, however it also displays several local maxima/minima in the valence/conduction band which are very close in energy. We have also noticed no sizable changes in the band dispersion near the gap region when varying slab thickness. In addition, the $BaSi_2$(101) and (110) slabs have multiple separate flat bands in the gap region (Fig. 3). Since the theoretically computed bulk band gap is estimated to be 0.83 eV, a significant reduction in the band gap for the slabs can be easily spotted. Thus, the $BaSi_2$(001), (110), and (101) slabs display 0.42, 0.45, and 0.50 eV, respectively, and these values are almost invariable with respect to the slab thickness except for the latter one. In the cases of the $BaSi_2$(010), (100), and (011) slabs the gaps get

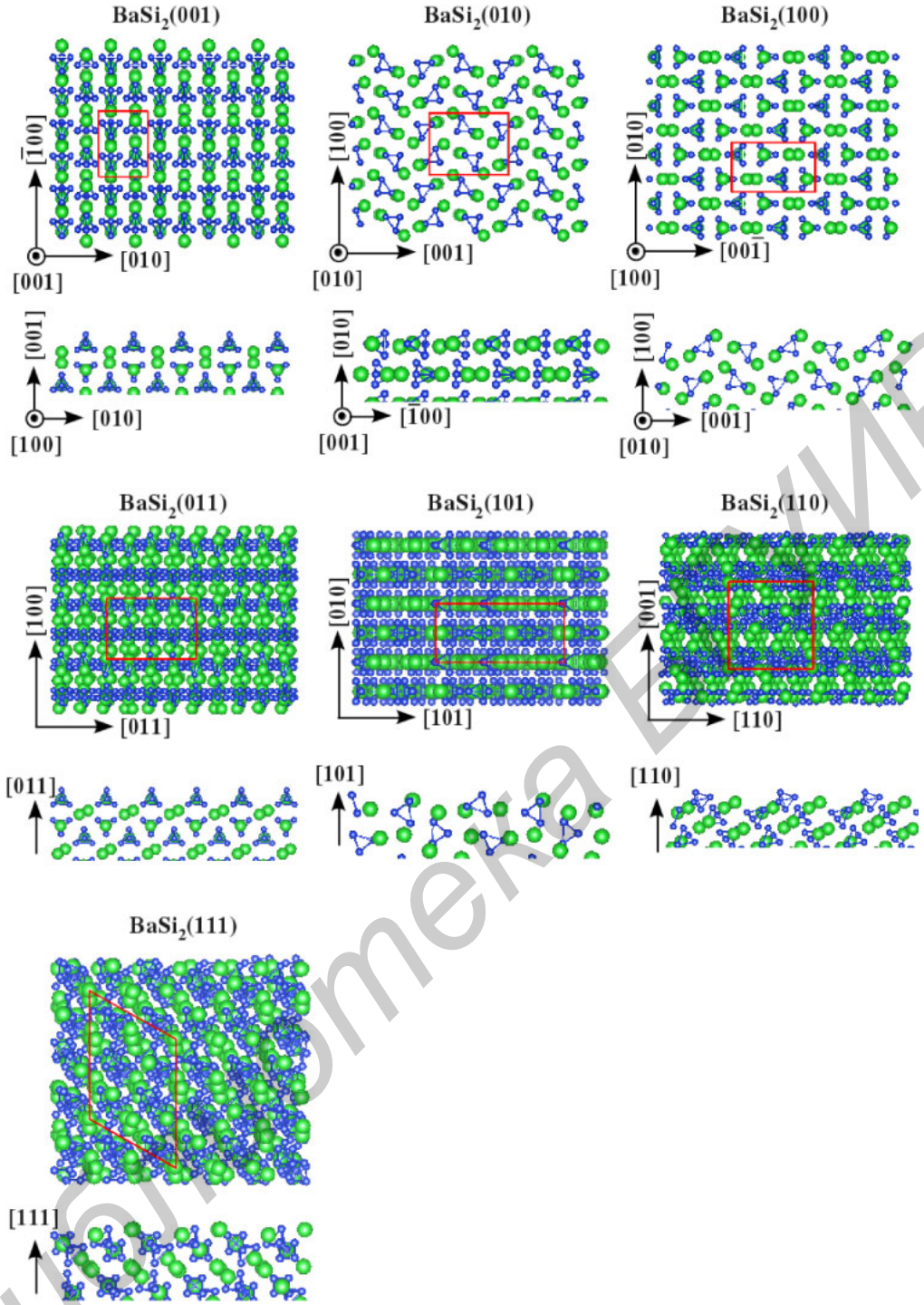

Fig. 2. (Color online) Top (top panels) and lateral (bottom panels) views of different surfaces of $BaSi_2$. Only a few layer are shown for lateral views. The large green spheres indicate Ba atoms while the small blue spheres stand for Si atoms. Crystallographic orientations are also indicated.

Table I. The surface energy (meV/Å^2) and position of hole (eV, above the bulk valence band maximum) and electron (eV, below the bulk conduction band minimum) states of different $BaSi_2$ surfaces.

Surface	Surface energy	Hole surface state	Electron surface state
(001)	40.0	One deep	One deep
(010)	29.0	One shallow	One shallow
(100)	29.3	No	One shallow at 0.05
(011)	40.0	One shallow	One shallow
(101)	34.6	Surface band at 0.43	No
(110)	40.1	Two deep	One shallow
(111)	28.8	No	No

larger (0.72, 0.81, and 0.73 eV, respectively) but they are still smaller than the one in the bulk and among them only the $BaSi_2$(100) slabs possess a well-pronounced dependence of gap changes on the slab thickness. Eventually, the $BaSi_2$(111) slab is characterized by the band-gap value of 0.87 eV to be larger than that in the bulk along with sizable band-gap variation with respect to slab thickness.

All considered $BaSi_2$ slabs are expected to be under the influence of quantum confinement effects which unavoidably should increase band-gap values. In order to explain the observed odd band-gap behavior in the slabs (band gaps which are smaller than in the bulk and almost invariable band

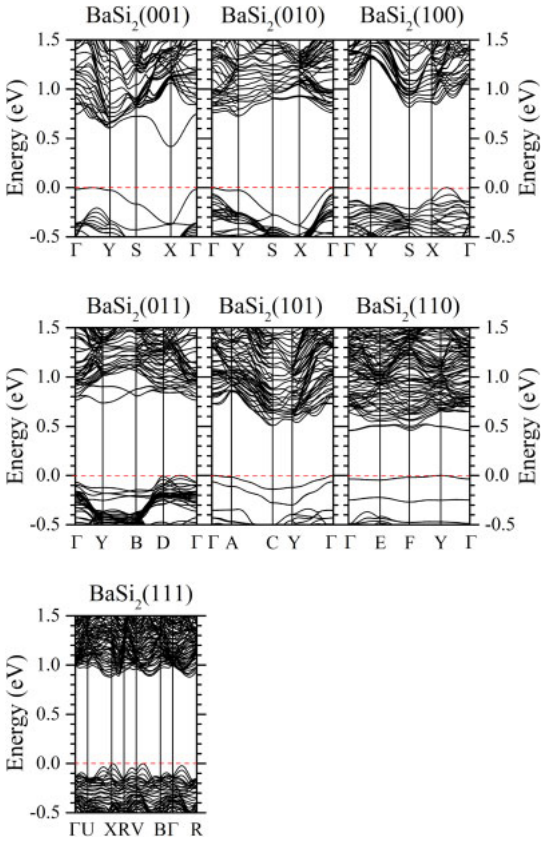

Fig. 3. (Color online) Band structures of $BaSi_2$ slabs with different orientations and thickness of about 5 nm. Zero at the energy scale corresponds to the top of the valence band. For the $BaSi_2$(001), (010), and (001) slabs the labeling of two-dimensional orthorhombic Brillouin zone corresponds to the projection of the three-dimensional orthorhombic Brillouin zone. For the $BaSi_2$(011), (101), and (110) slabs the corresponding labeling of two-dimensional monoclinic Brillouin zone are the following: G (0, 0), Y (0, 1/2), B (0.62, 1/2), D (0.62, 0), A (0, 0.51), C (1/2, 0.51), E (0.52, 1/2), F (0.52, 0). In the case of two-dimensional triclinic Brillouin for the $BaSi_2$(111) slab the labeling is: G (0, 0), U (0.48, −0.16), X (0.96, 0.58), R (0.47, 0.74), V (0.08, 0.91), B (−0.47, 0.16).

gaps with respect to the slab thickness) we have carefully analyzed the character of the states in band extrema points as well as in top valence bands and bottom conduction bands as presented in Fig. 4. For the $BaSi_2$(001) slabs the well-resolved maximum of the valence band is mainly characterized by Si-s and Si-p states of atoms which are located at the surface, while s-, p-, and d-states of surface Ba atoms define the minimum of the conduction band (see Fig. 4). For the $BaSi_2$(110) slabs several filled flat bands in the gap region are populated by Ba-d and Si-p states of atoms situated right at the surface, whereas the lowest in energy conduction band is mainly characterized by Ba-s, Ba-d, and Si-p states of the surface atoms however in the minimum of the conduction band there are some admixtures of states of atoms which are spread all over the slab. Similar behavior, when states of surface atoms solely define the extrema points, can be traced for the other slabs. In fact, Ba-d and Si-p states populate the maximum of the valence band in the $BaSi_2$(010) slabs; Ba-p, Ba-d, and Si-p, states dominate in the maximum of the valence band in the $BaSi_2$(101) slabs; Ba-s, Ba-d, Si-s, and Si-p states are present in the minimum of the conduction band in the $BaSi_2$(011) slabs. There are also cases when contributions to the extrema points are small and they originate from almost all atoms in a slab. This situation is typical of maximum of the valence band for the $BaSi_2$(011) slabs and of the minimum of the conduction band for the $BaSi_2$(100), (010), and (111) slabs. Finally, contributions coming from atoms, which are located primarily in the inner part of a slab, can be traced in the maximum of the valence band for the $BaSi_2$(100) and (111) slabs and in the minimum of the conduction band for the $BaSi_2$(101) slabs. Similar characters in extrema points have been already identified for different surfaces of Ca_2Si.[27)]

3.3 Quantum confinement and surface effects in $BaSi_2$ thin films

On the next step the band-gap dependence on the slab thickness was studied more thoroughly. The typical cases represented by the $BaSi_2$(100) and (001) thin films are depicted in Fig. 5(a). As the first feature one can trace a clear band-gap reduction to some limiting value with increasing $BaSi_2$ slab thickness due to the attenuation of the quantum confinement effects. This limiting value can be equal to the bulk band gap [for the $BaSi_2$(111) film]. But also this value can be slightly [for the $BaSi_2$(100) film] or significantly [for the $BaSi_2$(101) film] less then the bulk band gap. According to the second feature one can spot almost invariable band-gap values with increasing $BaSi_2$ slab thickness [for the $BaSi_2$(001), (010), (110), and (011) films].

To understand such a behavior of the band-gap dependence on film thickness the following two basic assumptions should be carefully considered. First of all the electron (hole) system, which is defined by electron (hole) states localized at atoms of the core region of a film, reproduces the energy levels affected by the so-called quantum confinement effects. Eventually, electron (hole) states localized at surface atoms reproduce the so-called surface states associated with energy levels, which are defined mainly by the surface nature but not by the quantum confinement effects.

Now let us recall what the so-called quantum confinement effects mean. The reduction in dimensionality in semiconducting nanostructures leads to drastic changes in the confined electron (hole) behavior. In the case of an isolated nanosized thin film, for example, one can consider that electrons (holes) are being placed in an infinite potential well. It results in additional quantum levels to appear for the particles. In this case the energy spectrum is described by the formula[30)]

$$E = \frac{\hbar^2 \pi^2 n^2}{2m^* d^2},$$

where $\hbar$ is the Planck's constant, m^* is the effective mass of particles, d is the well width, and n is the principal quantum number. Thus, within the standard effective mass approximation (EMA) the confined electrons (holes) are additionally upward (downward) shifted in energy [$\Delta E_e = (\hbar^2\pi^2)/(m_e^* d^2)$ and $\Delta E_h = (\hbar^2\pi^2)/(m_h^* d^2)$, respectively] with respect to the bulk (E_g^{bulk}) and the new band-gap value will be

$$E_g = E_g^{bulk} + \Delta E_e + \Delta E_h = E_g^{bulk} + \frac{\hbar^2\pi^2}{d^2}\left(\frac{1}{m_e^*} + \frac{1}{m_h^*}\right).$$

Recently, we proposed a model in order to explain similar behavior of the band gap in TiO_2 nanowires and nanotubes.[31,32)] It was assumed that for some nanostructures the

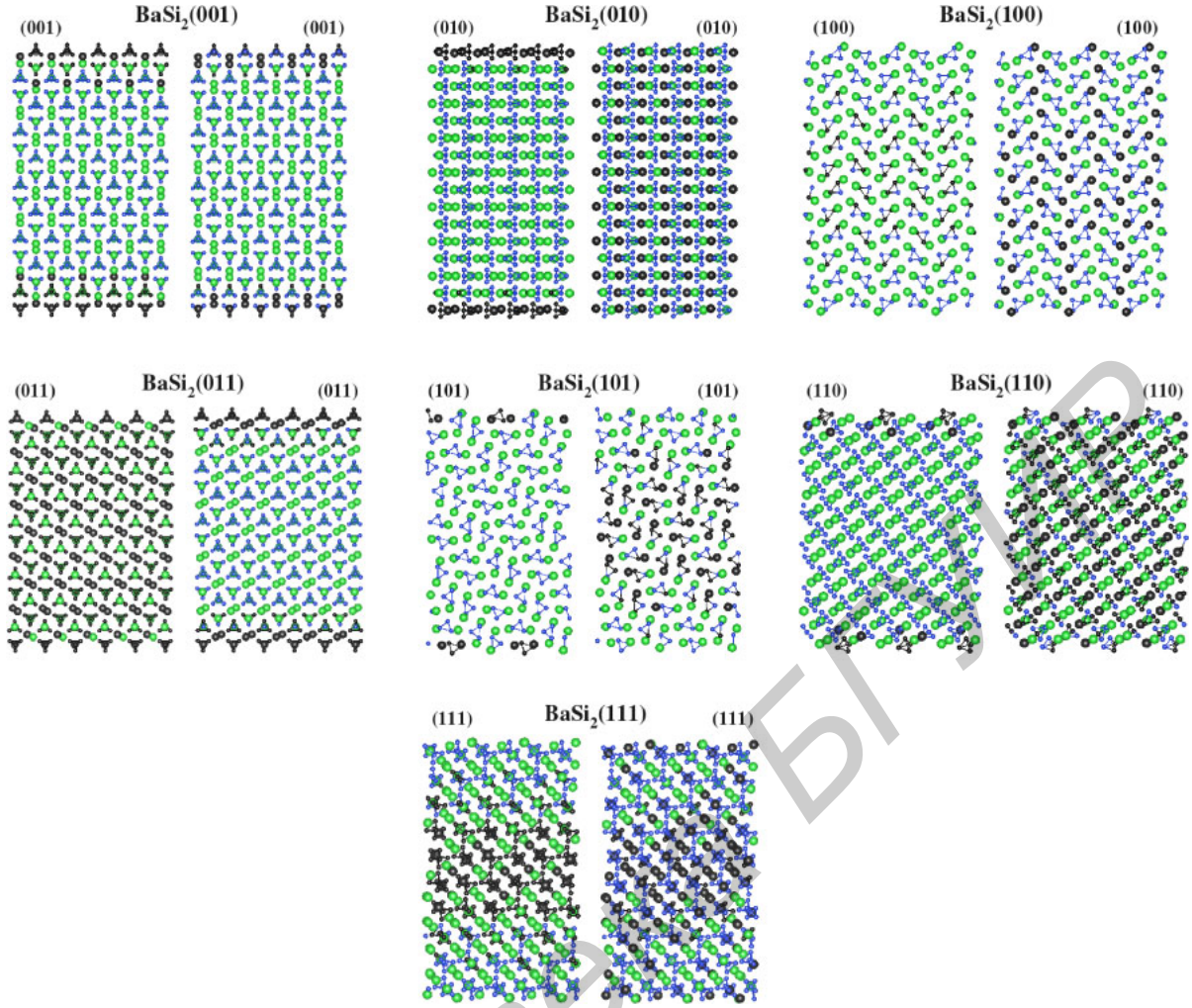

Fig. 4. (Color online) Lateral view of $BaSi_2$ slabs with different surfaces highlighting Ba (large, black spheres) and Si (small, black spheres) atoms whose states characterize the top of the valence band (the corresponding left panel) and the bottom of the conduction band (the corresponding right panel). The rest of the Ba and Si atoms are large, green and small, blue spheres, respectively.

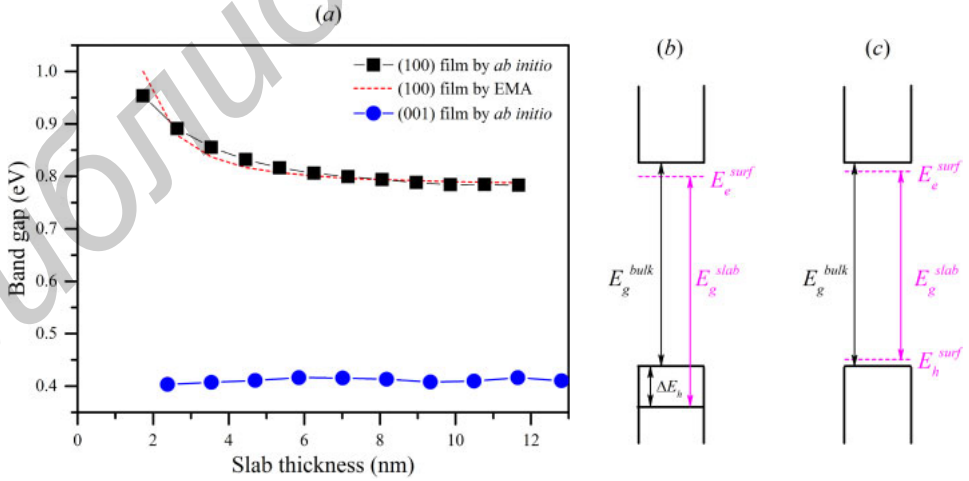

Fig. 5. (Color online) (a) The band-gap variation in the $BaSi_2$(100) and (001) slabs with respect to the their thickness along with the EMA fitting. (b) The schematic energy diagram of the $BaSi_2$(100) slabs indicating the energy gap of the bulk (E_g^{bulk}), the shift in energy of the holes due to the quantum confinement effects (ΔE_h), the energy of the surface electron states (E_e^{surf}) and the band gap of the slabs (E_g^{slab}). (c) The schematic energy diagram of the $BaSi_2$(001) slabs indicating the energy gap of the bulk (E_g^{bulk}), the energy of the surface hole (E_h^{surf}) and electron (E_e^{surf}) states and the band gap of the slabs (E_g^{slab}).

electron (hole) states which defined the appropriate minimum (maximum) of the conduction (valence) band can be treated as the surface states with the energy lying within the bulk band-gap region. Moreover, these surface states *do not* display a subsequent upward (downward) shift due to the quantum confinement effects.

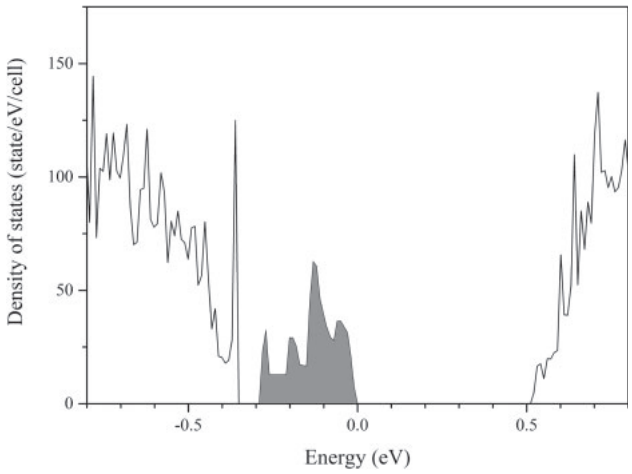

Fig. 6. The total density of states near the gap region of the $BaSi_2(101)$ slab with thickness of about 5 nm which band structure is shown in Fig. 3. Zero at the energy scale corresponds to the top of the valence band. The shadow area indicates the surface band.

For the case of the $BaSi_2(100)$ films, where the appearance of an electron state is possible according to the performed analysis of characters of the states in the band extrema points (Fig. 4), the band gap of the slab is defined as $E_g^{slab} = E_g^{bulk} - E_e^{surf} + \Delta E_h$ [see Fig. 5(b)]. Also we would like to stress a point that for real nanostructures often some deviation from the $\Delta E_g \sim 1/d^2$ law (in the case of an ideal infinite rectangular well) could be observed and the exponential power N in $\Delta E_g \sim 1/d^N$ can be considered, in general, as a fitting parameter. The best fit for the band-gap data in this case [Fig. 5(a)] was obtained for $m_h^* = 0.31m_0$, where m_0 is the free electron mass,[5] $N = 1.96$ and $E_e^{surf} = 0.05$ eV (i.e., the surface state is formed by the electrons and is situated below the bulk conduction band minimum). Applying the above analysis to the $BaSi_2(101)$ film and using the appropriate values of the effective mass for electrons one can find the $E_h^{surf} = 0.43$ eV (i.e., the surface state is formed by the holes and is situated above the bulk valence band maximum). For the $BaSi_2(111)$ film, no any surface states are formed and both the electron and the hole systems are affected by the quantum confinement effects.

To illustrate the situation for all of the rest considered cases, when the band-gap values stay almost still and can be defined by the difference between the electron and hole surface states, we present the schematic diagram in Fig. 5(c). The appropriate values for the band gap are 0.42, 0.45, 0.72, and 0.73 eV for the $BaSi_2(001)$, (110), (010), and (011) film, respectively. Unfortunately, one cannot definitely say where such energy levels corresponding to the surface electron and hole states should be placed on the diagram since the energy difference between these levels is only known. In the cases of the $BaSi_2(101)$ and (110) slabs multiple separate flat bands formed by surface states are clearly seen in the gap region (Fig. 3), while in the former one a hole surface band has evolved from surface states. It is evident in the corresponding density of states in Fig. 6 where the shadow area indicates the hole surface band.

4. Conclusions

Results of our ab initio calculations clearly indicate the $BaSi_2(111)$, (010), and (100) surfaces to be preferable in energy displaying rather low values of surface energies with respect to the other surfaces under investigation. In addition, we have revealed that the appearance of Ba atoms as the topmost surface atoms leads to sizable lowering in surface energy and to stabilization in the charge distribution among Si atoms forming Si_4 surface tetrahedra. The corresponding band structures of $BaSi_2$ thin films show all nanostructures to be semiconductors regardless of their orientation and film thickness. However, we have observed in some cases that values of band gaps are smaller than in the bulk and/or they are invariable when changing the film thickness. Such odd behavior was explained to the presence of surface states which define the top/bottom of the valence/conduction band and are not affected by quantum confinement effects. By employing a simple EMA model we could extract energy positions of the surface states for the $BaSi_2(100)$ and (101) surfaces: the shallow electron state at 0.05 eV (below the bulk conduction band minimum) and deep hole state at 0.43 eV (above the bulk valence band maximum), respectively. According to the corresponding band structures both shallow hole and electron states (<0.1 eV) are expected for the $BaSi_2(010)$ and (011) surfaces, while the $BaSi_2(001)$ ones are characterized by the presence of deep hole and electron states. For the $BaSi_2(110)$ surfaces two deep hole states and one shallow electron state are predicted. Eventually, no well-resolved surface states have been detected for the $BaSi_2(111)$ surfaces. Even though the EMA approach indicates the presence of deep hole state for the $BaSi_2(101)$ surfaces, the analysis of density of states clearly shows the formation of the surface band with the width of about 0.3 eV in the gap region. The detailed information on surface states for different surfaces of $BaSi_2$ is also summarized in Table I.

Acknowledgments

Dmitri B. Migas is grateful to the organizers of the Asia-Pacific Conference on Semiconducting Silicides and Related Materials Science and Technology 2016 (APAC-SILICIDE 2016) for a kind invitation, financial support and a nice opportunity to present recent results on silicides. The authors thank the Belarusian National Research Program "Convergence-2020", "Materials Science, New Materials and Technologies" and Belarusian Republican Foundation for Fundamental Research under (Grant No. F16R-048).

1) M. I. Fedorov and G. N. Isachenko, Jpn. J. Appl. Phys. **54**, 07JA05 (2015).
2) T. Suemasu, Jpn. J. Appl. Phys. **54**, 07JA01 (2015).
3) T. Nakamura, T. Suemasu, K. Takakura, F. Hasegawa, A. Wakahara, and M. Imai, Appl. Phys. Lett. **81**, 1032 (2002).
4) K. Morita, Y. Inomata, and T. Suemasu, Thin Solid Films **508**, 363 (2006).
5) D. B. Migas, V. L. Shaposhnikov, and V. E. Borisenko, Phys. Status Solidi B **244**, 2611 (2007).
6) K. Toh, T. Saito, and T. Suemasu, Jpn. J. Appl. Phys. **50**, 068001 (2011).
7) D. B. Migas and V. E. Borisenko, Phys. Status Solidi C **10**, 1658 (2013).
8) M. Kumar, N. Umezawa, and M. Imai, J. Appl. Phys. **115**, 203718 (2014).
9) M. Baba, K. Toh, K. Toko, N. Saito, N. Yoshizawa, K. Jiptner, T. Sakiguchi, K. O. Hara, N. Usami, and T. Suemasu, J. Cryst. Growth **348**, 75 (2012).
10) M. Baba, K. Watanabe, K. O. Hara, K. Toko, T. Sekiguchi, N. Usami, and T. Suemasu, Jpn. J. Appl. Phys. **53**, 078004 (2014).
11) K. O. Hara, N. Usami, K. Toh, M. Baba, T. Toko, and T. Suemasu, J. Appl. Phys. **112**, 083108 (2012).
12) K. O. Hara, N. Usami, K. Nakamura, R. Takabe, M. Baba, K. Toko, and T. Suemasu, Appl. Phys. Express **6**, 112302 (2013).

13) W. Du, M. Suzuno, M. Ajmal Khan, K. Toh, M. Baba, K. Nakamura, K. Toko, N. Usami, and T. Suemasu, Appl. Phys. Lett. **100**, 152114 (2012).
14) M. Kobayashi, Y. Matsumoto, Y. Ichikawa, D. Tsukada, and T. Suemasu, Appl. Phys. Express **3**, 021301 (2010).
15) S. Okasaka, O. Kubo, D. Tamba, T. Ohashi, H. Tabata, and M. Katayama, Surf. Sci. **635**, 115 (2015).
16) M. Baba, S. Tsurekawa, K. Watanabe, W. Du, K. Toko, K. O. Hara, N. Usami, T. Sekiguchi, and T. Suemasu, Appl. Phys. Lett. **103**, 142113 (2013).
17) D. Tsukahara, M. Baba, S. Honda, Y. Imai, K. O. Hara, N. Usami, K. Toko, J. H. Werner, and T. Suemasu, J. Appl. Phys. **116**, 123709 (2014).
18) M. Baba, K. O. Hara, D. Tsukahara, K. Toko, N. Usami, T. Sekiguchi, and T. Suemasu, J. Appl. Phys. **116**, 235301 (2014).
19) J. Evers, J. Solid State Chem. **32**, 77 (1980).
20) G. Kresse and J. Hafner, Phys. Rev. B **49**, 14251 (1994).
21) G. Kresse and J. Furthmüller, Phys. Rev. B **54**, 11169 (1996).
22) G. Kresse and J. Furthmüller, Comput. Mater. Sci. **6**, 15 (1996).
23) G. Kresse and J. Joubert, Phys. Rev. B **59**, 1758 (1999).
24) J. P. Perdew, S. Burke, and M. Ernzerhof, Phys. Rev. Lett. **77**, 3865 (1996).
25) W. Tang, E. Sanville, and G. Henkelman, J. Phys.: Condens. Matter **21**, 084204 (2009).
26) M. Kumar, N. Umezawa, and M. Imai, J. Alloys Compd. **630**, 126 (2015).
27) D. B. Migas, V. O. Bogorodz, A. B. Filonov, V. L. Shaposhnikov, V. E. Borisenko, and N. G. Galkin, Jpn. J. Appl. Phys. **54**, 07JA03 (2015).
28) H.-Y. Wang, X.-N. Xue, X.-Y. Xu, C. Wang, L. Chen, and Q.-C. Jiang, CrystEngComm **18**, 8599 (2016).
29) D. B. Migas, S. Cereda, F. Montalenti, and L. Miglio, Surf. Sci. **556**, 121 (2004).
30) P. Y. Yu and M. Cardona, *Fundamentals of Semiconductors Chemistry. Physics and Materials Properties* (Springer, Berlin, 2010) 4th ed.
31) D. B. Migas, A. B. Filonov, V. E. Borisenko, and N. V. Skorodumova, Phys. Chem. Chem. Phys. **16**, 9479 (2014).
32) D. B. Migas, A. B. Filonov, V. E. Borisenko, and N. V. Skorodumova, Phys. Chem. Chem. Phys. **16**, 9490 (2014).